Pediatrics Cardiovascular FDG-PET Imaging

21

Geneviève April, Sophie Turpin,
Raymond Lambert, and Joaquim Miró

Introduction

^{18}F-FDG PET/CT is well established in the pediatric population for both oncologic and nononcologic indications. Among them, cardiac ^{18}F-FDG PET/CT represents a very polyvalent and specific niche, with particular considerations in children. The aim of this chapter is to review the features, particularities, and applications of pediatric cardiac ^{18}F-FDG PET/CT imaging, including protocol optimization and its role in the investigation of Kawasaki disease and anomalous coronaries, infection, congenital heart disease, and pericardial disease.

Minimization of Radiation Exposure

Cardiac ^{18}F-FDG PET/CT, although uncommonly performed in children, can be helpful in various clinical contexts. It can, however, represent an additional source of ionizing radiation and must therefore be used responsibly [1]. The typical effective dose of an ^{18}F-FDG PET/CT study is 3.5–8.6 mSv (0.10–0.14 mCi/kg) for the PET component. For the CT component, the effective dose is 0.3–2.2 mSv for a low-dose attenuation correction CT and 2–10 mSv for diagnostic CT. Absorbed dose (mGy) and effective dose (mSv/mCi) are typically higher for small children and infants compared to teenagers and adults [2]. This is mainly due to a more compact anatomical disposition of organs and a higher radiosensitivity of tissues. Some strategies for dose optimization of ^{18}F-FDG PET/CT include the following [2–5]:

Eliminating Unnecessary Examinations

When imaging is considered necessary, the ordering physician should choose the best modality to appropriately answer the underlying clinical question. Important factors include availability, cost, diagnostic accuracy, radiation exposure, and feasibility in children while minimizing risks and discomfort. Referring physicians should be aware of the limitations and diagnostic yield of the chosen imaging modality. In cases where ^{18}F-FDG PET/CT is considered appropriate, it should follow the best technical standards in order to optimize the diagnostic yield of the test.

Reducing Radiotracer Dose

Harmonized consensus guidelines have been developed by the European Association of

G. April (✉) · S. Turpin · R. Lambert · J. Miró
CHU Ste-Justine, Montreal, QC, Canada
e-mail: Joaquim.Miro.med@ssss.gouv.qc.ca

© The Author(s), under exclusive license to Springer Nature Switzerland AG 2022

M. Pelletier-Galarneau, P. Martineau (eds.), *FDG-PET/CT and PET/MR in Cardiovascular Diseases*, https://doi.org/10.1007/978-3-031-09807-9_21

Nuclear Medicine (EANM) and the Society of Nuclear Medicine and Molecular Imaging (SNMMI) regarding optimal ^{18}F-FDG dosing in children. The 2021 guidelines recommend doses of 0.10–0.14 mCi/kg (3.7–5.2 MBq/kg) of ^{18}F-FDG for whole-body PET/CT imaging, with a minimum of 0.7 mCi (26 MBq) and a maximum of 10 mCi (370 MBq). The purpose of this weight-based dosing is to minimize radiation exposure without compromising diagnostic performance. A good overall strategy is to determine the longest reasonably achievable scan time per bed position and to adjust administered radiotracer activity accordingly [6, 7].

Optimizing CT Imaging Parameters and Reducing Scan Range

Diagnostic CT in pediatrics is considered more challenging than in adults mainly because of lower intrinsic soft tissue contrast in children. The CT component of an ^{18}F-FDG PET/CT study is used for attenuation correction purposes and anatomical localization and can provide additional tissue characterization when iodinated contrast agents are used. Factors affecting radiation dose delivered during a CT include tube current time product (mAs), beam energy (kVp), helical pitch, and axial collimation. Child-specific CT protocols reduce CT radiation exposure by decreasing mAs, reducing kVp, and increasing pitch. One suggested approach is to categorized CT acquisition parameters by weight range. Attention must be focused on optimal patient positioning, as off-center positioning increases peripheral and surface CT dose indexes (CTDI) by as much as 10–50% [8, 9]. In addition, CT parameters should be tailored to the area of the body imaged.

^{18}F-FDG PET/CT Protocols

Typical ^{18}F-FDG PET/CT Imaging Session

For a typical ^{18}F-FDG PET/CT session, the patient is installed in a dark, quiet room, with a warm blanket, with or without premedication, to avoid activation of brown fat metabolism. Patient weight, height, and blood sugar level are measured. A fasting period of 4–6 h is typically required, and dextrose infusions can be stopped 90 min before injection. The use of short-acting insulin should also be avoided at least 4 h before radiotracer injection. The uptake period following radiotracer injection varies depending on indication but is usually between 30 and 90 min. Before the acquisition, the patient is asked to void and/or the diaper is changed. Acquisitions usually last between 10 and 50 min. After imaging, hydration is recommended to minimize bladder radiation dose [10].

Myocardial Viability

The main goal of a viability protocol is to maximize heart glucose consumption. The corollary being that viable cardiomyocytes, including hibernating myocardium, maintain the ability to metabolize glucose. Bringing the patient into a hyperglycemic state stimulates insulin production and release, which promotes entry of glucose into cardiomyocytes. As opposed to adult myocardial viability preparation, pediatric patients do not need to fast prior to imaging and no insulin injection is required. After measurement of blood sugar level, an oral glucose solution (1.5 g/kg up to a maximum of 50 g) is given. After 45 min, blood sugar level is reassessed and ^{18}F-FDG is injected. Imaging takes place approximately 45 min following radiotracer injection. Should oral intake be impossible, an intravenous glucose (25% or 50%, 0.3 g/kg, over a period of 15 min) can be employed [11].

Myocardial Suppression

The main goal of a suppression protocol is to minimize physiological heart glucose consumption by favoring fatty acid metabolism. When appropriately suppressed, myocardial

glucose uptake should reflect inflammation or infection rather than physiological metabolism. Various suppression protocols emulating those used in adults have been proposed. These include a 24-h low-carbohydrate diet (including avoidance of dextrose infusion), a prolonged fast of 12 h or more, and administration of low-dose IV heparin 45 min (5 UI/kg IV) and 15 min (10 UI/kg IV) before ^{18}F-FDG injection. In breastfed or formula-fed infants, it is often not possible to perform a myocardial suppression study [12].

^{18}F-FDG PET/CT and Pediatric Sedation

Sedation is not a substitution for adequate child and parent preparation, as multiple nonpharmacologic strategies exist to help children cooperation. Optimization of the PET/CT or PET/MR environment is key. In neonates and infants, darker rooms, noise-reduction techniques, as well as feed-and-wrap techniques have been proven successful. In older children, the main goal is to decrease anxiety and to promote distraction using movies and music to reduce motion artifacts. Using these strategies, most ^{18}F-FDG PET/CT examinations can be performed without the use of sedation. However, in some cases, sedation remains necessary for reduction of patient motion, cooperation, and discomfort minimization considerations [13].

Sedation can be divided into conscious sedation, deep sedation, and general anesthesia, with some overlap between these levels of sedation. Patients who require more than conscious sedation necessitate appropriate monitoring. Risks associated with sedation include hypoventilation and apnea, airway obstruction, and sometimes morbidity related to gastrointestinal adverse effects, reactive airway disease, and risk of seizure [14].

Selecting the level of sedation should be made on a case-by-case basis. Guidelines recommend a minimum of 2 h of clear fluid fasting prior to elective procedures. However, prolonged fasting may be deleterious especially in infants. Therefore, ingestion of clear fluids up to 1 h before elective anesthesia or sedation is acceptable. Breastfeeding and milk preparations should be stopped 4 h, and solids minimally 6 h before procedure [15].

The choice of drugs and route of administration depends on multiple factors, including age, underlying comorbidities, institutional protocols, length and type of procedure, availability of reversal drugs, monitoring equipment and adequately trained practitioners to manage all levels of sedation [16]. The most frequently used sedative agents include chloral hydrate, phenobarbital sodium (Nembutal), midazolam, ketamine, dexmedetomidine, propofol, and nitrous oxide [17, 18].

Pediatric ^{18}F-FDG PET/MR Cardiovascular Imaging

Hybrid PET/MR systems offer several advantages in the pediatric population, allowing for the combination of PET functional information with the precise anatomical information and high-contrast structural resolution of MRI [19]. PET/MR does not require additional CT to perform attenuation correction or spatial coregistration, resulting in a more favorable dosimetry. However, whole-body PET/MR acquisitions are longer compared to a whole-body PET/CT and require optimal registration, which usually necessitates patient sedation. Furthermore, several devices such as pacemakers or mechanical heart valves, frequently present in children with congenital heart disease, are not MRI compatible or may lead to significant artifact. Finally, PET/MR is susceptible to artifacts related to field-of-view truncation, attenuation-correction, and motion [20, 21].

Cardiac MRI is technically challenging in children. Proper acquisition requires the use of

ECG gating, which may be technically challenging in infants with rapid heart rate or in patients with pacemakers. Sequences have to be adapted depending on the patient's ability to breathe hold and their size for proper contrast enhanced MRI angiography [22, 23]. When combined with MRI, respiratory gating of the PET component is possible, but the use of a respiratory belt remains more efficient than gating with MR-based navigators [24, 25].

In pediatric cardiology, potential applications of hybrid PET/MR include the evaluation of cardiac tumors and myopathies, where both modalities are complementary. In children for whom both PET and MRI are required, hybrid PET/MR allows imaging within a single session, minimizing discomfort and potentially avoiding additional sedation. Children could benefit from ^{18}F-FDG PET/MR for the evaluation of rare primary cardiac tumors or secondary invasion by either adjacent or metastatic neoplasms, with superior soft tissue characterization. PET/MR also provides anatomical precision for the evaluation of congenital cardiac abnormalities before surgery, as well as improved evaluation of soft tissue infection. PET/MR has the potential to assess flow, metabolism, and cardiac function in conditions such as Kawasaki disease, aberrant coronary arteries, and for the differentiation of ischemic and nonischemic cardiomyopathies. It can also be combined with ^{18}F-FDG for viability assessment, delineation of scar tissue by late gadolinium enhancement (LGE) imaging, identification of fat content, tissue edema and inflammation, as well as infiltrative diseases such as myocarditis [26, 27].

Kawasaki Disease

Kawasaki disease (KD) is an acute systemic vasculitis of unknown etiology. It affects mainly small and medium-sized arteries including the coronary arteries. When coronary arteries are involved, KD can lead to major complications such as acute myocardial infarction (AMI). It is one of the most frequent acquired heart diseases in children, especially in North America and Japan [28]. Classic KD presentation includes ongoing fever for 5 days or more, and at least 4 of the 5 following clinical features: mucosal changes, polymorphous exanthema, nonexudative conjunctivitis, skin alteration of the extremities, and lymphadenopathy.

Even with optimal treatment, which includes aspirin and intravenous immunoglobulins, coronary artery aneurysms and stenosis are relatively frequent in KD. While half to two-thirds of KD-induced coronary aneurysms regress spontaneously, some, mainly giant aneurysms (>8 mm), tend to persist and are associated with an increased risk of complications. Regression of lesions is more frequent in younger children, females, and in more distally located aneurysms. Approximately one-third of moderate-size lesions persist beyond 3 years after onset. Overall, coronary artery sequelae occur in approximately 20–25% of cases [29]. Since KD sequelae often present as multivessel disease, coronary revascularization is often necessary. A combination of a perfusion study, using ^{99m}Tc SPECT agents or PET tracers (e.g. NH_3 and ^{82}Rb), along with a ^{18}F-FDG PET viability study can be performed to evaluate viable myocardium (Fig. 21.1) [30].

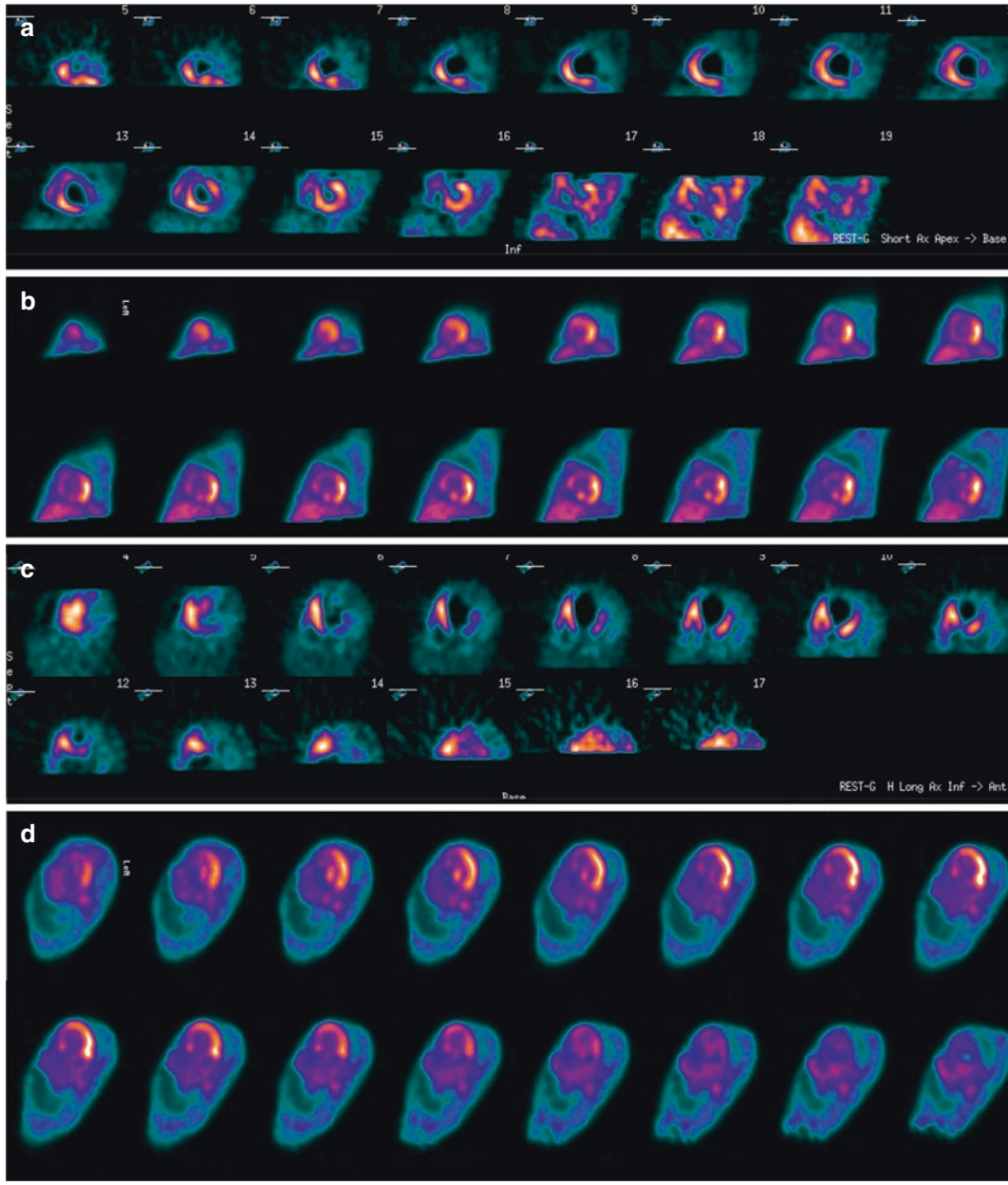

Fig. 21.1 ^{18}F-FDG PET/CT of a 5-year-old girl with a previous history of Kawasaki disease complicated by coronary aneurysm admitted with acute myocardial infarct. Tc99m myocardial rest perfusion study demonstrated extensive defects involving the anterior, anterolateral, and apical regions both on vertical short axis (**a**) and horizontal long axis (**c**). Post procedure evaluation of residual viable myocardium with ^{18}F-FDG PET/CT after glucose loading demonstrated myocardial hibernation and thus viability in the anterior, anterolateral, and apical regions both on vertical short axis (**b**) and horizontal long axis (**d**)

Anomalous Coronaries

Anomalous coronaries can be isolated or found in association with other cardiac malformations. Several classifications have been proposed based on the affected coronary, location of the anomalous origin, as well as its course in relation to the aorta and main pulmonary artery [31–33]. Native coronary anomalies are found in approximately 0.2–1.2% of the population [34, 35].

Anomalous origin of the left coronary artery from the pulmonary artery (ALCAPA) is a relatively prevalent congenital anomaly, usually seen as an isolated lesion and affecting 0.25–0.5% of the population. It is a well-known cause of myocardial ischemia and infarction in children and, if left untreated, can result in a mortality rate of up to 80–90% within the first year of life [36]. The typical clinical presentation, known as Bland–White–Garland syndrome, includes pallor, failure to thrive, sweating, and atypical chest pain while eating or crying. Neonatal pulmonary vascular resistance is high and pulmonary artery (PA) pressure ensure antegrade flow from the PA into the anomalous left coronary. With time, as pulmonary vascular resistance decreases, there is a consequent decrease in left coronary artery antegrade flow, with eventual reversal resulting in left-to-right shunting into the PA, causing the so-called coronary steal [37]. Infants have essentially no collateral circulation, leading to the rapid onset of severe myocardial ischemia, left ventricular dysfunction, and possible mitral valve regurgitation from papillary muscle ischemia. ALCAPA must be suspected in any infant or child presenting with myocardial dysfunction. Surgical correction is usually performed as soon as possible, regardless of age and degree of collateralization.

Imaging of coronary anomalies relies mainly on coronary computed tomographic angiography (CCTA), transthoracic echocardiography, and MRI [38, 39]. Perfusion and myocardial viability studies using PET can be used to assess for the presence of hibernating myocardium, which may influence surgical management in patients with massive infarction or aneurysm. Absence of viable tissue may indicate the need to consider heart transplant over revascularization. Resection of nonviable aneurysms may prevent malignant arrhythmias from developing and help prevent myocardial remodeling. Children with hibernating myocardium often show a significant recovery of function following revascularization. As well, mitral insufficiency frequently regresses after revascularization. Quantifying the amount of viable myocardium can also help predict surgical outcomes and the need for mechanical support bridging, as well as orienting postoperative follow-up [30].

Congenital Heart Disease

Congenital heart disease (CHD) is one of the most frequent congenital disorders and a leading cause of mortality associated with birth defects. Global prevalence of CHD is estimated to be 8 per 1000 live births. With improvement of surgical and medical management, survival is now possible for most patients, even with serious anomalies, although many patients have significant complications during adulthood. Approximately two third of adults with CHD eventually die from a cardiac cause, mainly heart failure and sudden death. Predictors of unfavorable prognosis are CHD severity, endocarditis, arrhythmias, myocardial infarction, and pulmonary hypertension [40]. As surgical techniques and patient survival continue to improve, more patients with repaired CHD may present with complications in adulthood. Thus, knowledge of the basic anatomy and physiology of CHD is critical for all cardiovascular imagers. The following sections provides a brief overview of the most frequent CHD and procedures.

Transposition of the Great Arteries

In transposition of the great arteries (TGA), the aorta and pulmonary artery connect to the inappropriate ventricles. In the majority of cases, this is an isolated anomaly, leading to profound cya-

nosis shortly after birth. The anatomy of the coronaries with regard to origin, proximal course, and branching is variable. One-year life expectancy without surgery is lower than 20%. Primary arterial switch operation is currently the treatment of choice. This intervention needs to be performed early in life, while the left ventricle is still exposed to high pressures and involves translocation of the coronary arteries to the neoaorta.

Single Ventricle and Hypoplastic Left Heart Syndrome

Univentricular CHD malformations are characterized by hypoplasia or absence of one of the ventricles or cardiac valves, leading to the impossibility of establishing normal serial circulation. The most severe form is hypoplastic left heart syndrome (HLHS), characterized by multiple levels of stenosis/hypoplasia of the structures of the left heart, and associated with aortic and mitral stenosis or atresia. As a consequence, the ascending aorta and aortic arch are hypoplastic, and systemic circulation is dependent on a patent ductus arteriosus. Other univentricular CHDs include double outlet right ventricle in which both the aorta and pulmonary artery arise from the right ventricle; hypoplastic right heart, the most severe form being secondary to tricuspid atresia; and the rare double inlet ventricle in which both atria are connected to a single ventricle. Univentricular CHD requires multiple staged surgical interventions to achieve serial circulation with one ventricle pumping the systemic circulation, while the pulmonary circulation depends on venous pressure, without any active pump (i.e. Fontan physiology).

Modified Blalock–Taussig Shunt

The modified Blalock–Taussig (BT) shunt is a palliative technique which uses a prosthetic graft to connect a subclavian artery to the ipsilateral pulmonary artery. It is commonly used in the neonatal period to augment pulmonary flow and relieve cyanosis, allowing the pulmonary arteries to grow and pulmonary resistances to drop, before corrective surgery or further palliation.

Bidirectional Glenn (Cavobipulmonary) Shunt

Bidirectional Glenn shunt is a palliative procedure which creates a shunt from the superior vena cava to the pulmonary arteries, in order to supply blood flow after neonatal pulmonary pressures have normalized. It is frequently used as a staging procedure in children with single-ventricle morphology who will eventually get a Fontan procedure. It results in one-half (from superior vena cava) of the systemic venous return going directly to the lungs, while the other half from the inferior vena cava returns directly to the heart.

Norwood Staged Procedures

The Norwood staged palliation for HLHS consists of three interventions. The first stage, performed shortly after birth, reestablishes an unobstructed systemic circulation using the right ventricle. To achieve this, the main pulmonary artery is transected and used to enlarge the hypoplastic aortic arch (the Damus–Kaye–Stansel procedure) (Fig. 21.2). The interatrial septum is excised to allow unobstructed pulmonary venous return to the systemic (right) ventricle. Since the pulmonary arteries are not connected to the right ventricle, an alternative source of pulmonary blood flow must be created, either by a modified BT shunt or a small conduit between the right ventricle and pulmonary arteries (Sano conduit) (Fig. 21.3). The second stage of the Norwood palliation consists of a bidirectional Glenn and is performed typically around 6 months of age, when pulmonary resistances have decreased. The third stage consist of a Fontan procedure, where the inferior vena cava is

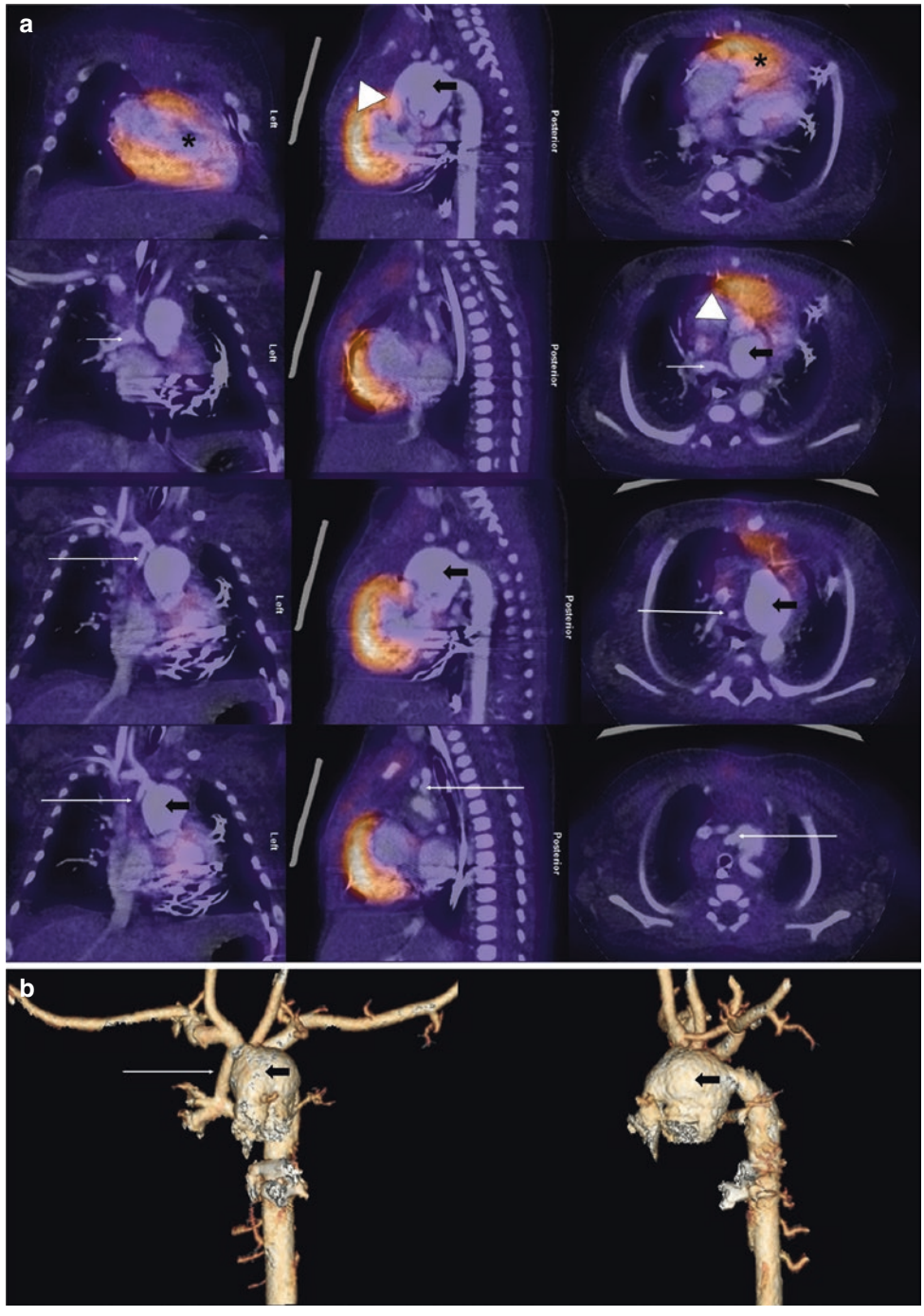

Fig. 21.2 ^{18}F-FDG PET/CT of a 1-month-old patient with left ventricle hypoplasia (*). ^{18}F-FDG CTAC images were fused with cardiac CT with contrast (**a**) and three-dimensional cardiac CT reconstructions (**b**). Norwood procedure with a Blalock–Taussig (BT) shunt (long thin arrow) between the right subclavian artery and right pulmonary artery (short thin arrow). Damus–Kaye–Stansel (DKS) procedure for creation of the neoaorta, with anastomosis of the main pulmonary artery (open arrow) and hypoplastic native aorta (arrow head)

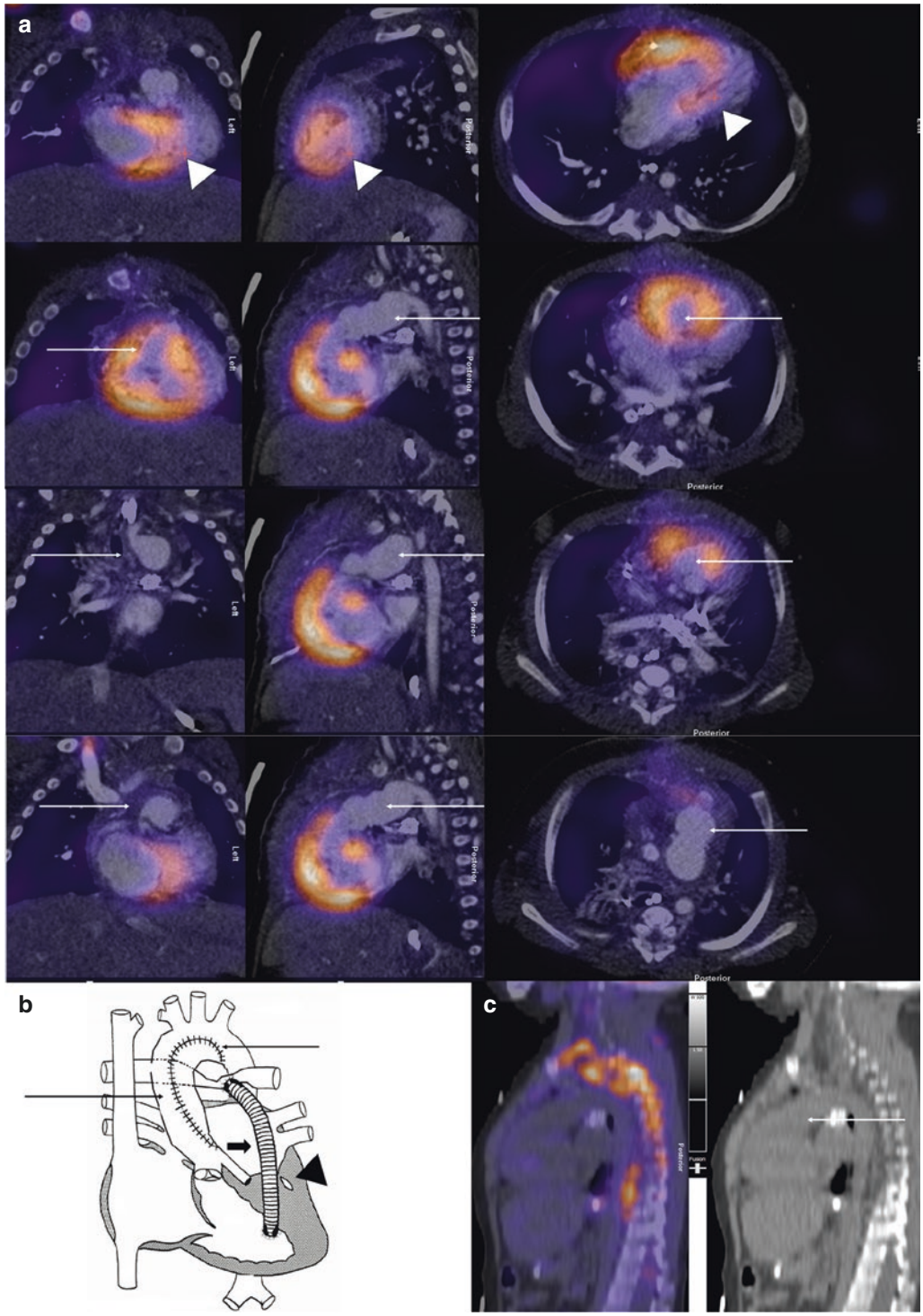

Fig. 21.3 ^{18}F-FDG PET/CT performed in a 2-year-old girl with left ventricular and aortic hypoplasia, status post Norwood–Sano procedure. ^{18}F-FDG CT AC images fused with: cardiac CT with contrast (**a**), cardiac catheterization image (**b**) and sagittal FDG CTAC PET/CT (**c**). Visible reconstructed aortic arch (long thin arrow), Sano shunt (open arrow) and hypoplastic left ventricle (arrowhead). When interpreting ^{18}F-FDG PET/CT, specifically in children with congenital heart disease, correlation with other modalities is paramount

connected to the pulmonary artery. Following this last stage, all deoxygenated blood from the venous system flows through the lungs. This last step is typically executed around 4 years of age, when the pulmonary arteries are mature enough to accommodate a large conduit [41].

Jatene Arterial Switch Procedure

This is the anatomical repair of transposition of great arteries performed to establish the left ventricle as the systemic arterial ventricle. If not possible in the neonatal period, it can sometimes be preceded by pulmonary artery banding, which places prosthetic material encircling the main pulmonary artery to "train" the left ventricle for systemic pressures.

Right Ventricle–Pulmonary Artery (RV-PA) Conduit

This technique uses, among different options, a valved prosthetic homograft material to create an artificial conduit between the right ventricle and pulmonary artery. Different surgical corrections can use this technique as a reconstruction of the right ventricular outflow tract (Fig. 21.4).

Tetralogy of Fallot

Although tetralogy of Fallot (ToF) and truncus arteriosus are distinct cyanotic congenital heart defects, they share some common characteristics. Both are a consequence of abnormal embryonic conotruncal development. They include a large septal defect at the ventricular outlet, with characteristic abnormalities of semilunar valves and great arteries. To be classified as ToF, CHD must fulfill specific requirements, including pulmonic stenosis, ventricular septal defect, overriding aorta, and right ventricular hypertrophy which represents a consequence of long-standing right ventricular pressure overload.

ToF are usually repaired using infundibulectomy and a patch repair of the RV outflow stenosis, which may involve the pulmonary valve. In cases where the pulmonary valve must be excised, a free pulmonary insufficiency is created, which may require future revalvulation. ToF repair frequently involves patch enlargement of the small pulmonary arteries, and even unifocalization, when the arteries are not in continuity (in this case, the pulmonary flow may come from aorto-pulmonary collaterals) or an RV-PA conduit. Complete ToF repair also involves closure of the ventricular septal defect using a patch allowing for septal realignment (Fig. 21.5).

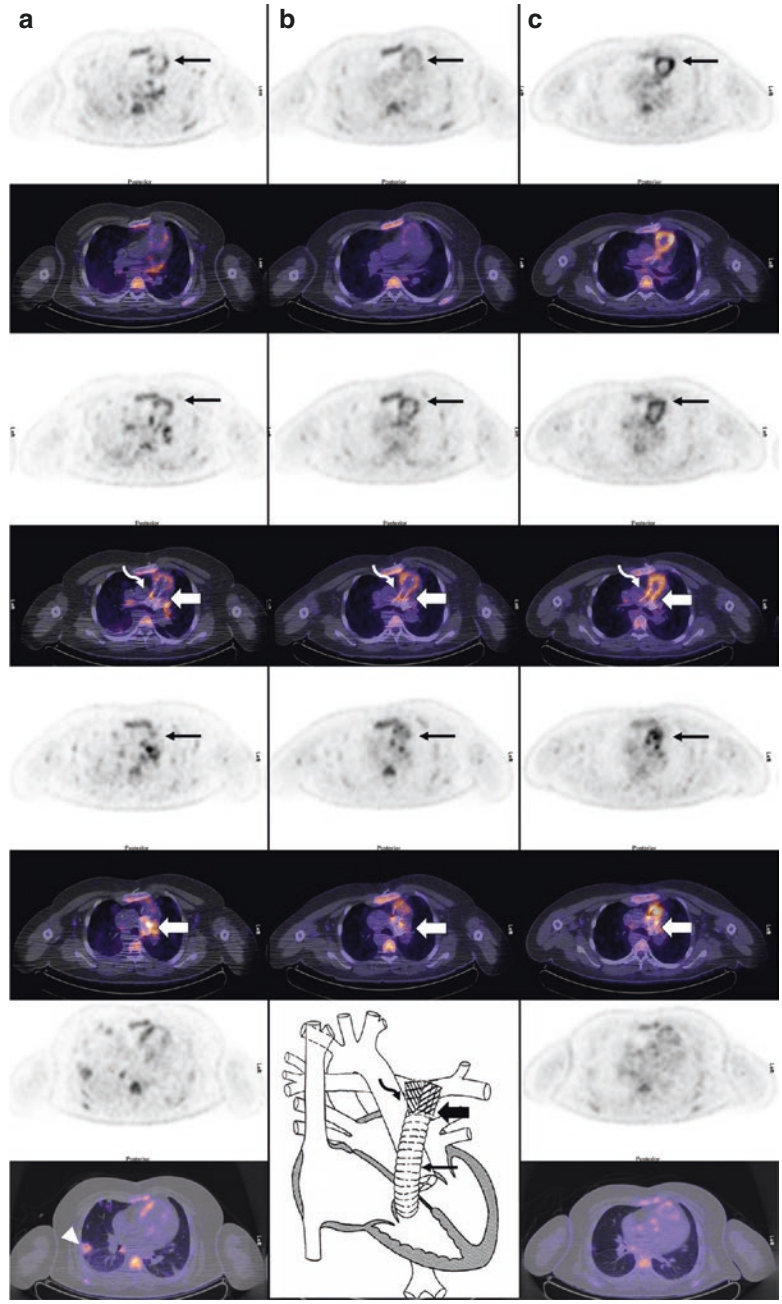

Fig. 21.4 ^{18}F-FDG PET/CT performed after a cardiac suppression protocol to assess extension of infection in a 15-year-old patient with truncus arteriosus status post RV-PA conduit (thin arrow), RPA (curvilinear arrow) and LPA (open arrow) stent placement. Clinically, the patient presented with *Staphylococcus aureus* septic shock following a toe infection. ^{18}F-FDG PET/CT demonstrating an active infectious process at the level of the RV-PA conduit, RPA and LPA stents, with lung septic emboli (arrow head) (**a**). Following 3 weeks of antibiotics, some improvement was noted (**b**), but during the following 2 weeks, despite aggressive antimicrobial treatment, the patient remained afebrile with increased inflammatory markers. A follow-up ^{18}F-FDG PET/CT study showed no further improvement at the levels of the LPA and RPA stents and progression of uptake surrounding the RV-PA conduit. Only resolution of the lung lesions was demonstrated (**c**). Shortly after, RV-PA conduit and both stents were surgically removed. Multiple vegetations, abscesses and *Staphylococcus aureus* were found on the material. A new RV-PA conduit was installed, the antibiotic treatment completed and patient's subsequent evolution was favorable

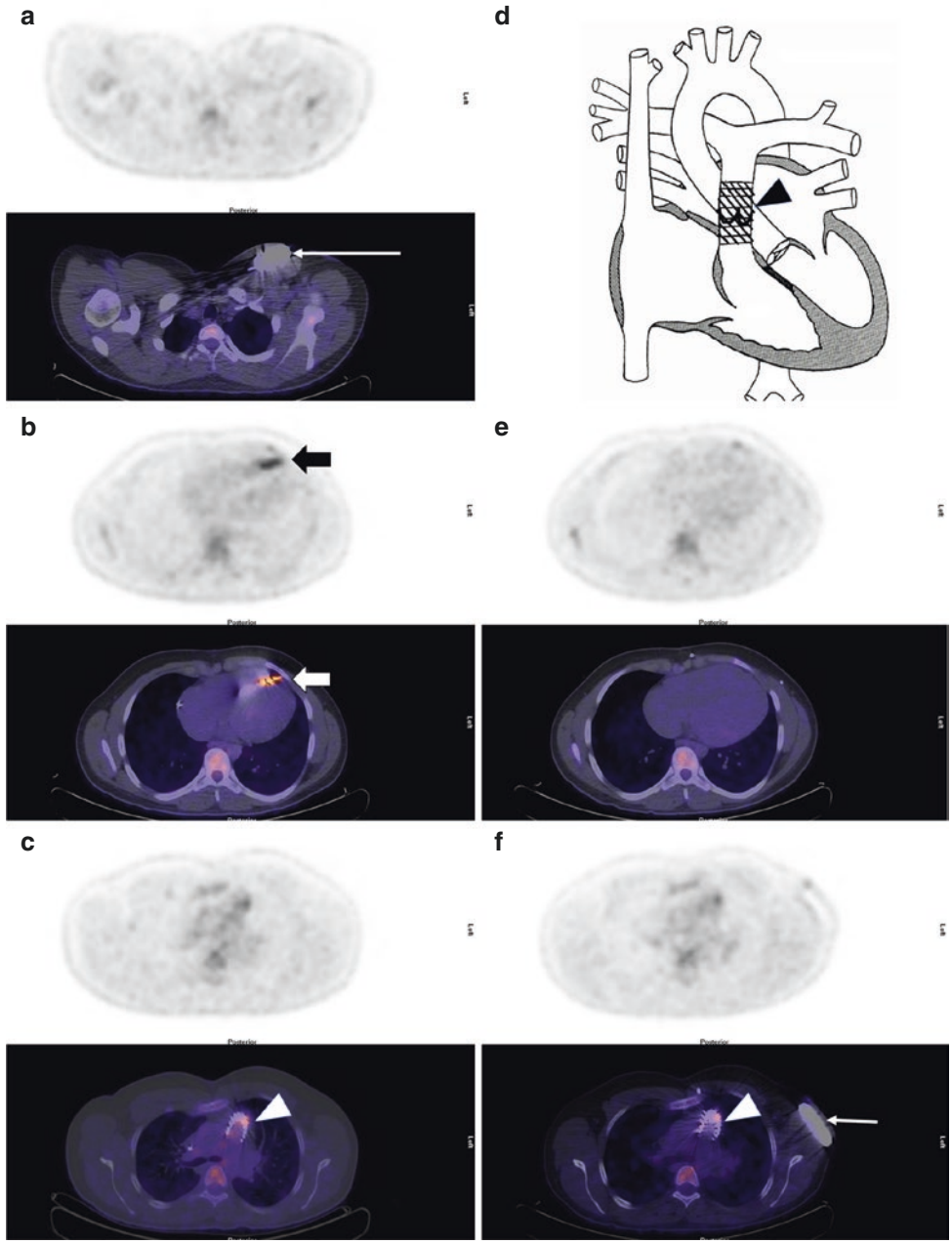

Fig. 21.5 ^{18}F-FDG PET/CT performed after cardiac suppression protocol to assess the extent of infection in a 16-year-old patient status post Fallot tetralogy repair. Status post stent placement Main Pulmonary Artery with Melody valve; status post Fortify Assura cardioverter defibrillator device (CDD) implantation. Follow-up echocardiogram showing vegetations at the level of the intracavitary apical defibrillation lead. No FDG uptake around was seen at the casing (long thin arrow) (**a**) but there was visible FDG uptake at the level of the defibrillation lead (short thick arrow) (**b**). Mild uptake at the level of the Melody valve (arrow head) but otherwise no FDG uptake at the level of the stent (**c**, **d**). The CDD was removed and cultures were positive for *Staphylococcus hominis*. Following antibiotic therapy, a second ^{18}F-FDG PET/CT showed resolution of uptake in the left ventricle (**e**) and unchanged appearance of the Melody valve (arrow head) (**f**). No evidence of persistent infection during follow-up. New subcutaneous implantable defibrillator (EMBLEM MRI S-ICD) (short thin arrow)

Cardiovascular Infections

In 2013, a joint European Association of Nuclear Medicine (EANM)/Society of Nuclear Medicine and Molecular Imaging (SNMMI) guideline recommended the use of ^{18}F-FDG PET/CT in inflammation and infection indications such as sarcoidosis, peripheral bone osteomyelitis, suspected spinal infection, fever of unknown origin (FUO), metastatic infection of high-risk patients with bacteremia, and primary evaluation of vasculitis [42]. The latest joint collaboration of the EANM and European Association of Cardiovascular Imaging (EACVI) published in 2020 now includes interpretation and reporting criteria of prosthetic valve endocarditis, cardiac implantable electronic devices, left ventricular assist device, and vascular graft infections [43]. However, these guidelines mainly apply to the adult population and pediatric-specific literature and recommendations remain scarce.

Infections Related to Sternotomy

Delayed sternal closure after cardiac surgery is a common technique in pediatric cardiac surgery, when sternal closure can negatively affect cardiac and respiratory function in the immediate postoperative period. Factors associated with increased infection risks are prolonged skin barrier disruption, prolonged mechanical ventilation/sedation/neuromuscular blockade, complex surgical intervention, younger age, and repeated surgery. Although antibiotic prophylaxis and wound dressing care reduces infection rates, infections including mediastinitis have been reported in between 4 and 10% of patients and ^{18}F-FDG PET/CT can be useful for the evaluation of suspected infection [44–46].

Congenital Heart Disease Repair

Surgical repair of CHD also often requires prosthetic material, which can be a predisposing factor for infection. In addition to the sternotomy site, multiple sites of infection are possible, including prosthetic conduits, native or prosthetic valves, and cardiac implantable devices. Infectious endocarditis (IE) prevalence is higher in patients with CHD. The reliability of the modified Duke criteria, including echocardiography findings, is limited due to artifacts and complex anatomy. Imaging is critical, not only for diagnosis, but also for the evaluation of response to therapy. The latest guidelines have incorporated ^{18}F-FDG PET/CT findings as a major criterion in the diagnostic algorithms for IE. ^{18}F-FDG PET/CT is also useful for the demonstration of extracardiac complications of endocarditis. Specifically, it allows for the detection of concomitant or alternative infective thoracic foci, such as pericardial collections, mediastinitis, and pulmonary infections (Fig. 21.6). Endocarditis can be associated with septic emboli, with extracardiac foci of infection reported in 15–60% [47–51].

Fever of Unknown Origin

Fever is one of the chief complaints of children presenting at the hospital, estimated to account for 16–30% of cases. FUO refers to a prolonged febrile condition without an established etiology despite complete evaluation, and no definite cause is found in 10–20% of cases. Although no widespread consensus exists, most current definitions of FUO in children include: temperature $\geq$ 38.3°C for >1 week, no history of immunosuppression in the preceding 3 months, with no clear cause identified despite complete physical examination, labo-

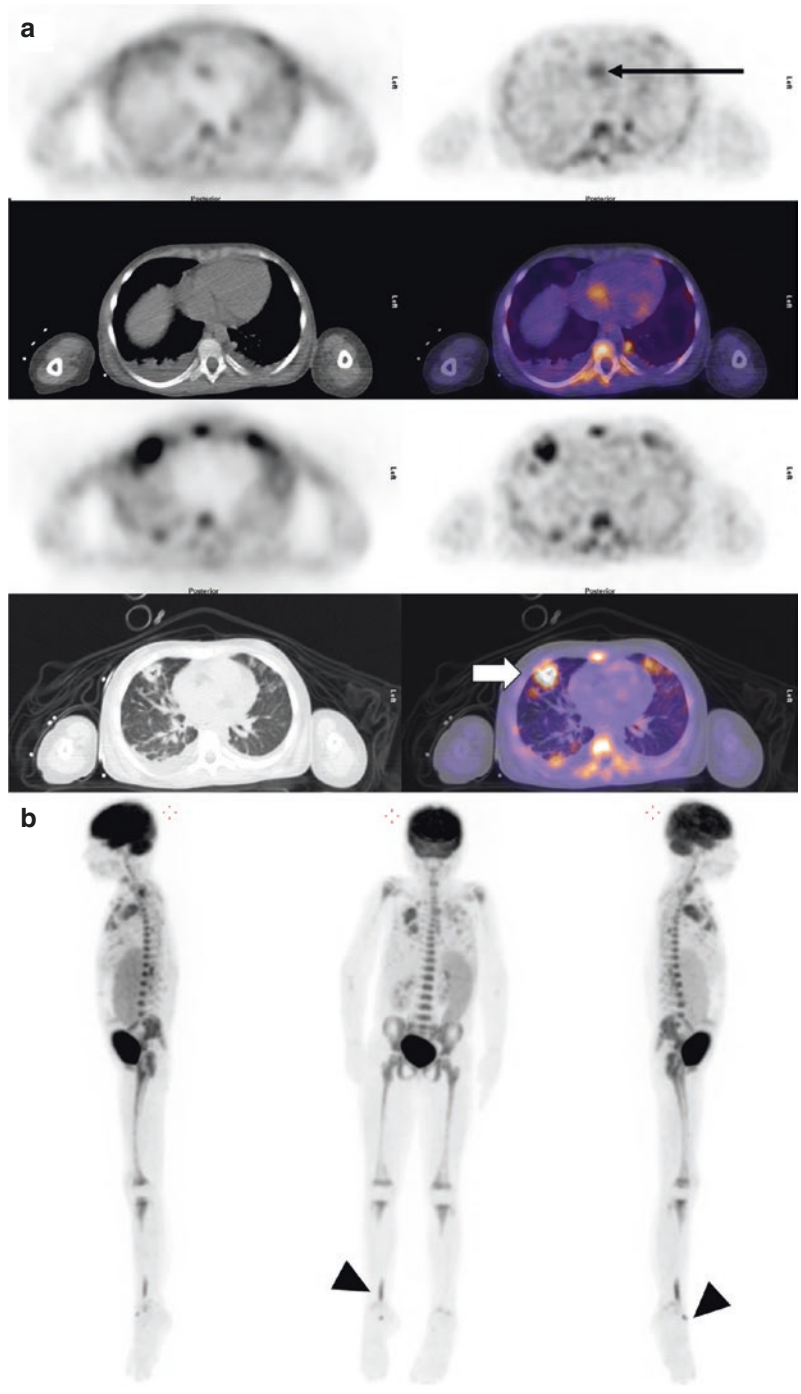

Fig. 21.6 ^{18}F-FDG PET/CT of a 10-year-old patient with indwelling central catheter for intravenous hyperalimentation admitted for septic shock. Tricuspid valve endocarditis and lung septic emboli were demonstrated on echocardiogram and chest CT. ^{18}F-FDG PET/CT was requested for the evaluation of left hip pain and performed with myocardial suppression protocol. Selected axial images (**a**) and Maximum Intensity Projections (**b**). FDG uptake was noted at the level of the tricuspid valve (long thin arrow). Lung septic emboli were present, some with cavitation (open arrow). Residual activity is seen at the FDG injection site (arrow head). No hip anomaly or other focus of infection was detected. The patient was known for splenomegaly

ratory and imaging workup. Causes of FUO include infection, malignancy, inflammatory disease, and other miscellaneous causes. ^{18}F-FDG PET/CT was found to have high sensitivity for several causes such as tumor (>90%), infection (89%), arthritis and vasculitis (65%), and is generally considered helpful in almost half of cases (25–75%), including chronic low-grade infections. ^{18}F-FDG PET/CT has good diagnostic accuracy in FUO, with reported sensitivity of ~85%, specificity of ~80%, PPV of ~70–85% and NPV of ~80–90%. ^{18}F-FDG PET/CT leads to modification of treatment in approximately half of cases, and has also proven useful in immunosuppressed children [52–54].

Ventricular Assist Devices

Infection affects nearly 15–20% of patients within a year of ventricular assist device (VAD) implantation, with infection at the driveline exit site seen most frequently. If isolated, the driveline can be debrided and revised, and the infection treated with antibiotics. Infection extending to internal components is associated with a high mortality rate and needs to be treated more aggressively. ^{18}F-FDG PET/CT has been shown useful in detecting infection of VADs in the adult population, with a pooled sensitivity of 92% and specificity of 83%, resulting in management changes in as much as 80% of patients [55–58] (Fig. 21.7).

Cardiac Implantable Electronic Devices

Cardiac Implantable Electronic Device (CIED) infections can present with superficial incisional infection, pocket infection, infection of thoracic leads, and endocarditis. Although less than 1% of all CIED are implanted in children, there are unique characteristics of the devices used in children. For instance, pacemaker stimulation is epicardial in smaller patients or patients with cavopulmonary connections, and the implantation chamber is often tunneled to the left upper abdominal quadrant (Fig. 21.8). Device dependence is more frequent with certain CHD (e.g., atrioventricular discordance), after open heart surgeries performed near the atrioventricular or the sinus node, and after complex heart surgeries, cardiomyopathies, or malignant ventricular arrhythmias. ^{18}F-FDG PET/CT enables diagnosis of infection, assessment of the extracardiac portion of leads, and localization of septic emboli foci. ^{18}F-FDG PET/CT is particularly effective in differentiating superficial tissue infection from deep pocket CIED infections requiring surgical excision (Fig. 21.9). A recent meta-analysis revealed a pooled sensitivity of 96% and pooled specificity of 97% for local pocket infection. Accuracy was slightly lower for lead infection, with a pooled sensitivity of 76% and specificity of 83% [59, 60].

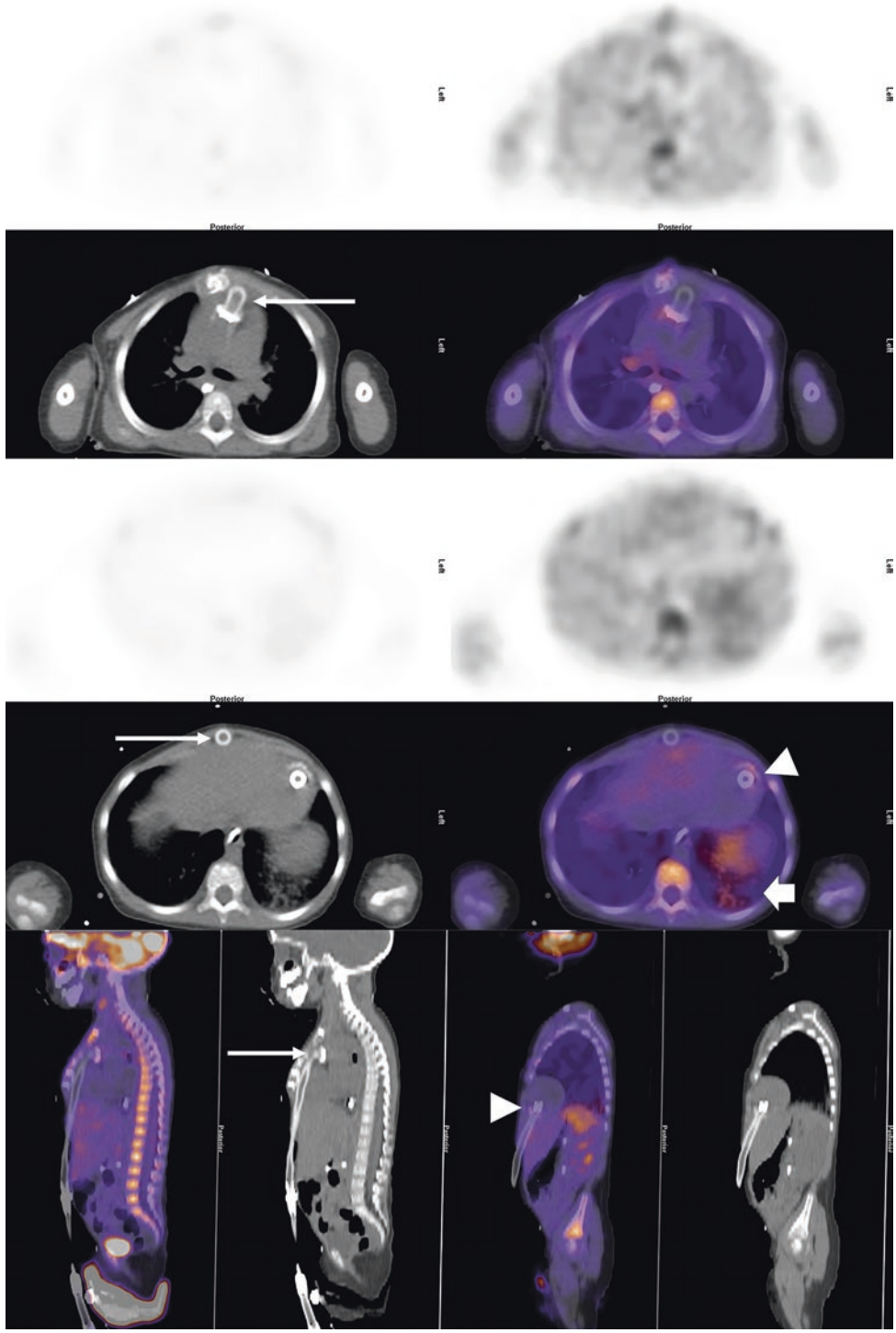

Fig. 21.7 ^{18}F-FDG PET/CT was performed in a 1.5-year-old girl with a history of recurrent fever and known Berlin Heart, a left ventricular assist device (LVAD). There was evidence of pneumonia in the left lung base (open arrow). There was physiologic radiotracer distribution associated with arterial cannula in the ascending aorta (long arrow) and atrial cannula in the left ventricle (short arrow), without evidence of material infection

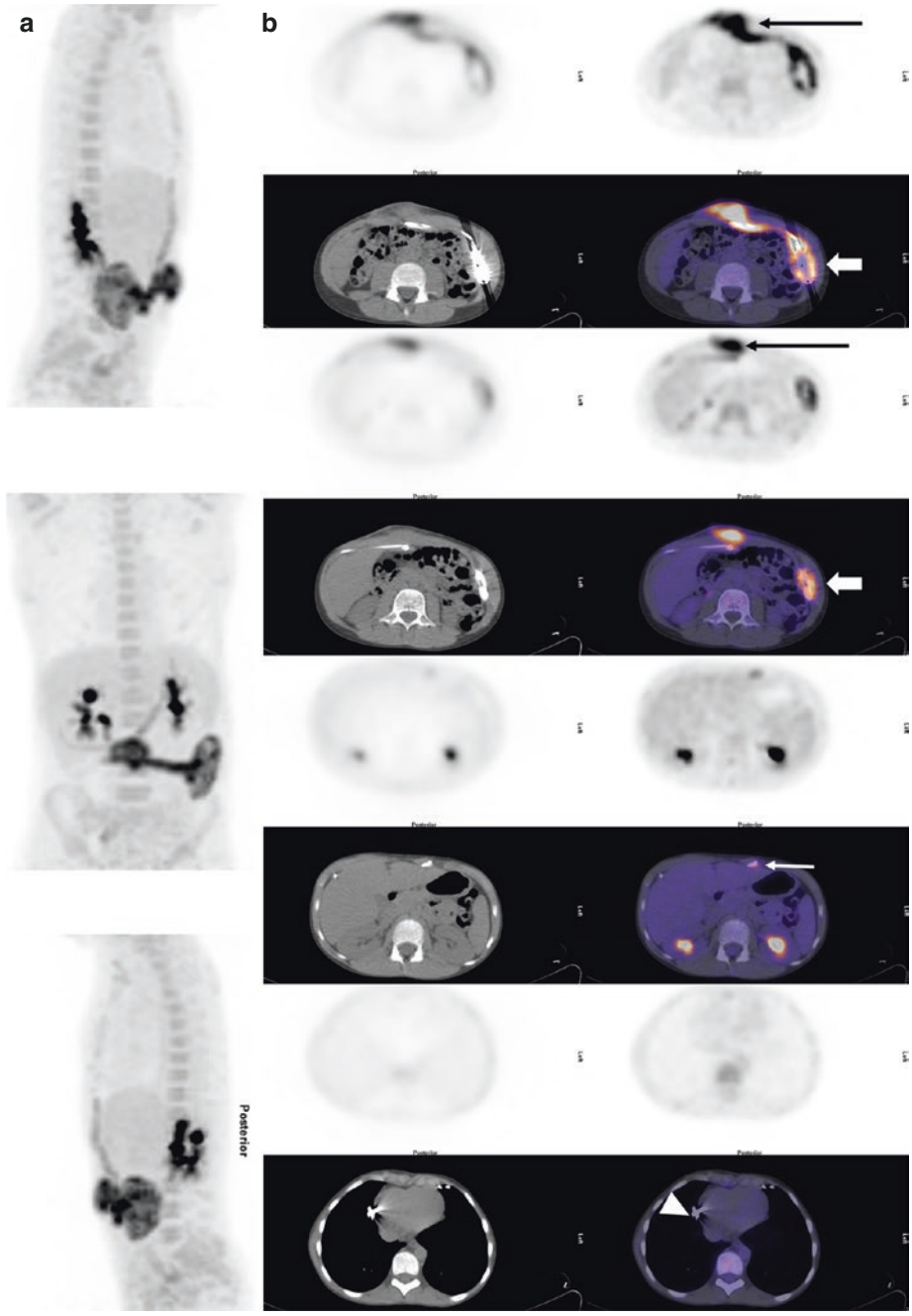

Fig. 21.8 ^{18}F-FDG PET/CT of a 9-year-old patient hospitalized for low-grade fever and induration in the epigastric region. The patient had multiple cardiac surgeries for congenital heart disease (double outlet right ventricle) including an epicardial dual chamber pacemaker implantation with implantable pulse generator in the left upper abdominal quadrant for third-degree atrioventricular block. After an inconclusive ultrasound of the latter region, ^{18}F-FDG PET/CT was performed: Maximum Intensity Projections (**a**) and selected axial images (**b**). Increased activity was found on both the non–attenuation-corrected (NAC) and CT attenuation-corrected (CTAC) images around the pacemaker casing (open arrow) and along the tunneled wires (long thin arrow). However, there was no supradiaphragmatic extension to the wires (thin short arrow) or to the epicardial leads (arrowhead). The pacemaker was removed and infection was confirmed. After a course of antibiotics with the patient under external pacing, a new pacemaker was installed, with no further complications

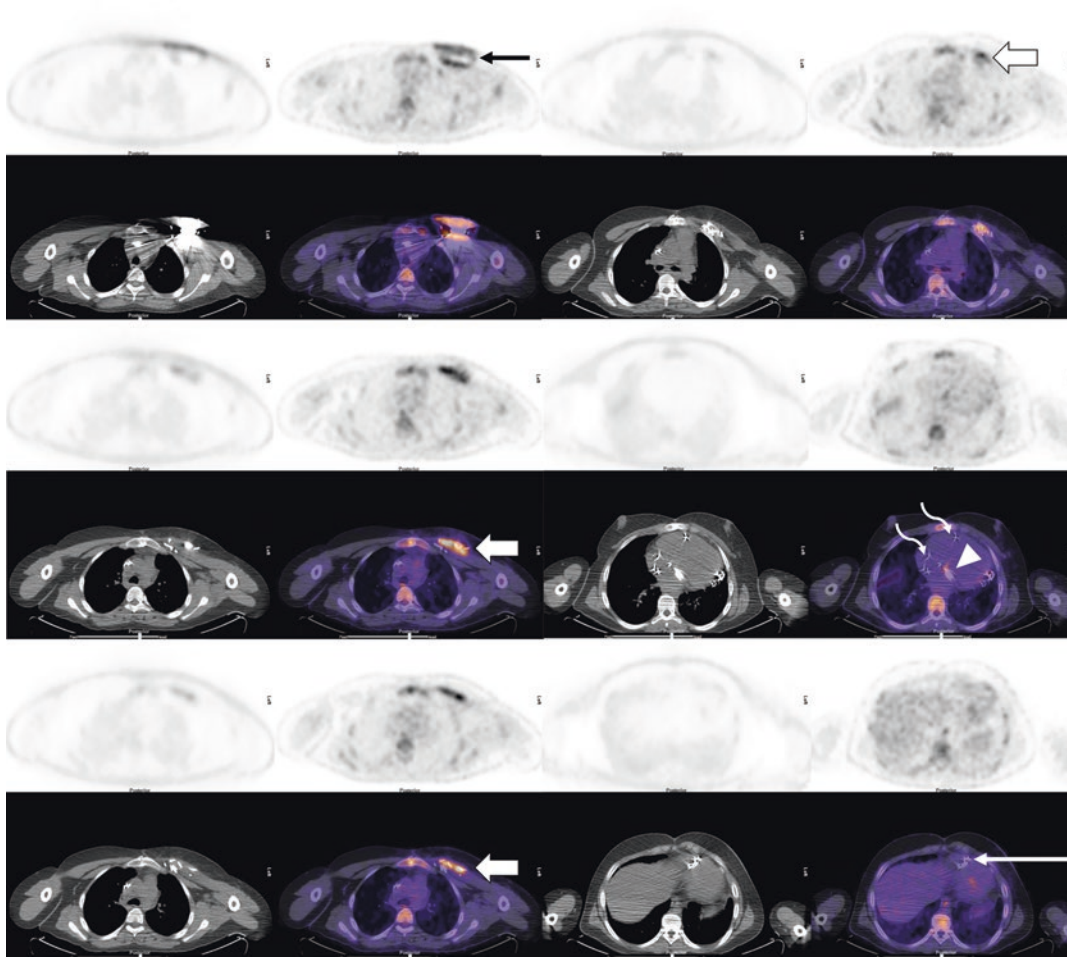

Fig. 21.9 ^{18}F-FDG PET/CT of a 15-year-old patient status post atrioventricular defect and coarctation of the aorta repair, post epicardial dual chamber pacemaker (ICD) implantation, and artificial mitral valve insertion. ICD replacement with three endovascular leads and one epicardial lead. There was a known superficial infection around the casing in the left hemithorax secondary to *Staphylococcus hominis*. As leads could not be properly visualized on echocardiogram, ^{18}F-FDG PET/CT with myocardial suppression protocol was performed. An active infectious process was demonstrated around the ICD casing (short thin arrow) and superficial wires (open arrow). No abnormal uptake was found at the level of the mitral valve (arrow head), endocardial leads (curvilinear arrows) or epicardial lead (long thin arrow). The patient underwent pacemaker extraction. After a course of antibiotics under external pacing, a new pacemaker was installed, without further complication

Pericardial Disease

Pericardial disease can be categorized as infectious versus noninfectious, and malignant versus nonmalignant. Etiologies include infectious, neoplastic, autoimmune, metabolic, iatrogenic, and traumatic causes. More often than not, the cause remains elusive [61]. The standard workup for pericarditis includes a thorough history, physical examination and additional investigations such as electrocardiogram, transthoracic echocardiography, and dosage or serum inflammatory biomarkers. ^{18}F-FDG PET/CT can play a role by assessing the activity of the pericardium and/or pericardial effusion (Fig. 21.10). In addition, whole body ^{18}F-FDG PET/CT can identify patterns of uptake suggestive of either infection, collagen vascular disease or neoplasm [62, 63]. Optimal imaging using myocardial suppression protocols should always be used.

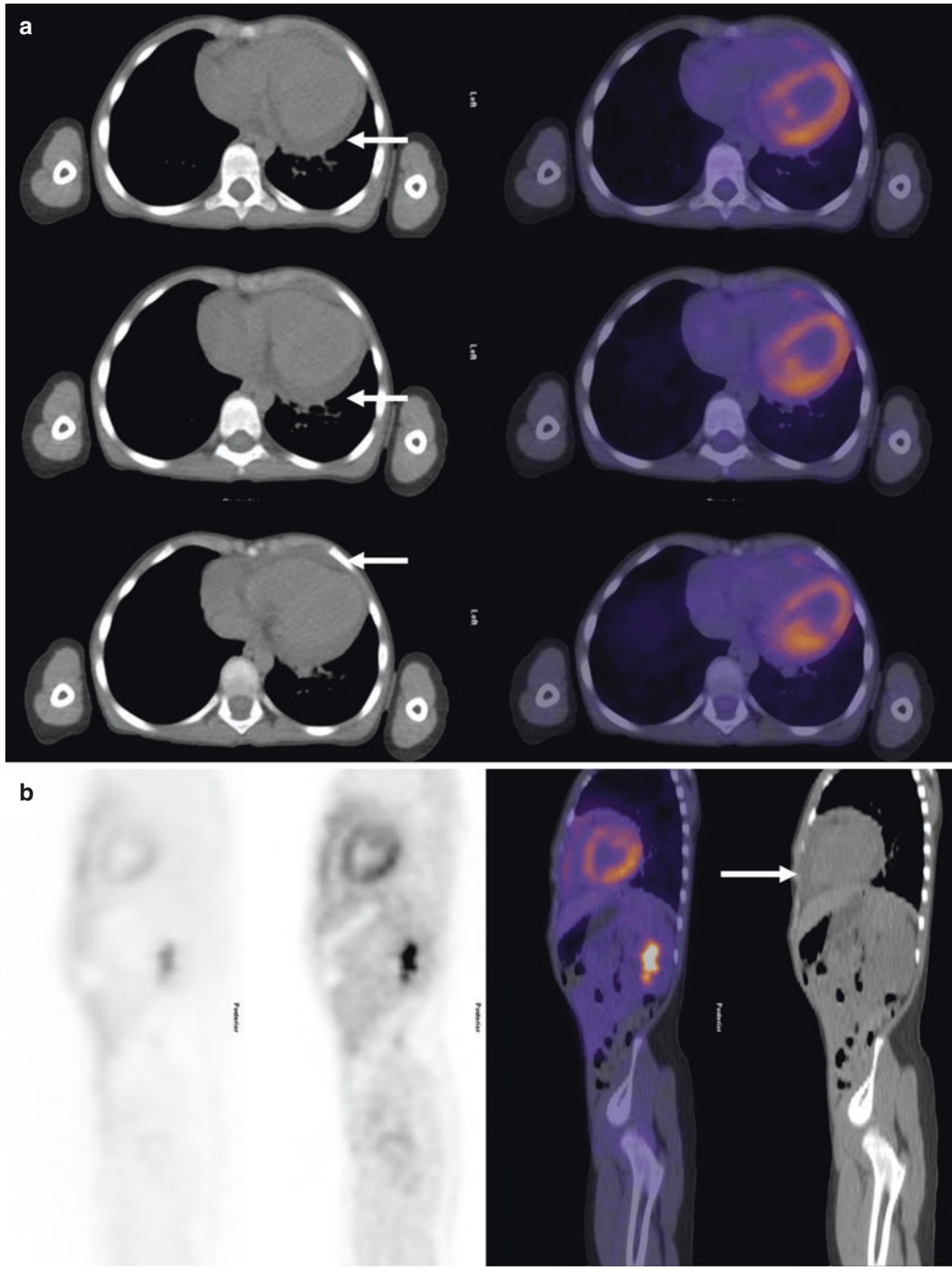

Fig. 21.10 ^{18}F-FDG PET/CT of a 5-year-old patient with a history of Kawasaki disease who presented with acute chest pain and heart palpitations. An echocardiogram demonstrated a pericardial effusion. ^{18}F-FDG PET/CT was requested to rule out collagen vascular disease as a clinical cause. Axial (**a**) and sagittal (**b**) images show significant pericardial effusion (arrow) with mild and diffuse uptake. The remaining study was normal. Biomarkers were negative. The final diagnosis was idiopathic pericarditis, which responded well to steroids

In neoplastic pericardial disease, ^{18}F-FDG PET/CT can help differentiate primary involvement of the pericardium from a paraneoplastic syndrome. Whereas direct involvement can originate from primary or metastatic malignancy, the most common underlying causes are different in children compared to adults. Hodgkin's lymphoma, especially bulky mediastinal disease, remains a frequent cause [63, 64]. Less frequently, other primary pericardial neoplasms such as sarcomas can be encountered [63]. Pericardial disease, especially when effusion is present, justifies investigation for an underlying malignancy.

Infectious pericardial disease etiologies include viral, bacterial, fungal, and rarely parasitic, with viral pericarditis being most frequent and often isolated. Apart from a viral prodrome, it resembles idiopathic pericarditis. It is usually not severe and has a good prognosis, although can be associated with a higher risk of myocardial damage [65]. ^{18}F-FDG PET/CT remains helpful for local evaluation of disease, along with cardiac MRI for the assessment of myocardial inflammation. It can also help detect septic emboli related to disseminated infection, which can change clinical management.

^{18}F-FDG PET/CT can be especially helpful for the investigation of tuberculous pericarditis. If left untreated, this condition can be associated with high morbidity and mortality. ^{18}F-FDG PET/CT can be helpful for the identification of pulmonary, bone, or colic foci, which can suggest the presence of underlying tuberculous infection and provide guidance for biopsy sampling [66, 67]. ^{18}F-FDG PET/CT can also help characterize constrictive pericarditis, associated with irreversible chronic inflammation and fibrosis of pericardium. Underlying causes can be idiopathic, postsurgical, postinfectious, or related to connective tissue diseases. Documenting active pericardial inflammation is helpful in the management of transient constrictive pericarditis [68].

Conclusion

Cardiac ^{18}F-FDG PET/CT in children has emerged as a useful tool allowing investigation of different pathologies affecting specific pediatric populations, such as those with congenital heart disease. Adapting nuclear medicine imaging and tailoring existing protocols to pediatric needs and adequate patient preparation depending on specific clinical indications ensures efficient and safe use of ^{18}F-FDG PET/CT in children, with minimization of adverse effects.

References

1. Edwards KW. Preparation and logistic considerations in performing PET and PET/computed tomography in pediatric patients. PET Clin. 2020;15(3):285–92.
2. Fahey FH, Goodkind A, MacDougall RD, Oberg L, Ziniel SI, Cappock R, et al. Operational and dosimetric aspects of pediatric PET/CT. J Nucl Med. 2017;58(9):1360–6.
3. Paiva FG, do Carmo Santana P, Mourao AP. Dosimetric study of pediatric PET/CT scan using different phantoms. Radiat Phys Chem. 2020;173:108887.
4. Parisi MT, Bermo MS, Alessio AM, Sharp SE, Gelfand MJ, Shulkin BL. Optimization of pediatric PET/CT. Semin Nucl Med. 2017;47:258–74.
5. Fahey FH, Goodkind AB, Plyku D, Khamwan K, O'Reilly SE, Cao X, et al. Dose estimation in pediatric nuclear medicine. Semin Nucl Med. 2017;47:118–25.
6. Treves ST, Gelfand MJ, Fahey FH, Parisi MT. 2016 update of the north American consensus guidelines for pediatric administered radiopharmaceutical activities. J Nucl Med. 2016;57(12):15N–8N.
7. Vali R, Alessio A, Balza R, Borgwardt L, Bar-Sever Z, Czachowski M, et al. SNMMI procedure standard/EANM practice guideline on pediatric 18F-FDG PET/CT for oncology 1.0. J Nucl Med. 2021;62(1):99–110.
8. Alessio AM, Kinahan PE, Manchanda V, Ghioni V, Aldape L, Parisi MT. Weight-based, low-dose pediatric whole-body PET/CT protocols. J Nucl Med. 2009;50(10):1570–8.
9. Turpin S, Abikhzer G, Lambert R. Simplified weight-based, low dose pediatric F18-FDG PET/CT protocols: dosimetry. J Nucl Med. 2011;52(supplement 1):1389.
10. McQuattie S. Pediatric PET/CT imaging: tips and techniques. J Nucl Med Technol. 2008;36(4):171–8.

11. Knuuti MJ, Nuutila P, Ruotsalainen U, Saraste M, Härkönen R, Ahonen A, et al. Euglycemic hyperinsulinemic clamp and oral glucose load in stimulating myocardial glucose utilization during positron emission tomography. J Nucl Med. 1992;33(7):1255–62.
12. Osborne MT, Hulten EA, Murthy VL, Skali H, Taqueti VR, Dorbala S, et al. Patient preparation for cardiac fluorine-18 fluorodeoxyglucose positron emission tomography imaging of inflammation. J Nucl Cardiol. 2017;24(1):86–99.
13. Schultz ML, Niescierenko M. Guidance for implementing pediatric procedural sedation in resource-limited settings. Clin Pediatr Emerg Med. 2019;20(2):116–22.
14. Mandell GA, Majd M, Shalaby-Rana E, Gordon I. Society of nuclear medicine procedure guideline for pediatric sedation in nuclear medicine. J Nucl Med. 2003;44:173–4.
15. Rosen D, Gamble J, Matava C. Canadian pediatric anesthesia society statement on clear fluid fasting for elective pediatric anesthesia. Can J Anesth. 2019;66(8):991–2.
16. Toney M, Pattishall S, Garber M. The time is now: standardized sedation training for pediatric hospitalists. Pediatrics. 2020;145(5):e20200446.
17. Sivaramakrishnan G, Sridharan K. Nitrous oxide and midazolam sedation: a systematic review and meta-analysis. Anesth Prog. 2017;64(2):59–65.
18. Eberson CP, Hsu RY, Borenstein TR. Procedural sedation in the emergency department. J Am Acad Orthop Surg. 2015;23(4):233–42.
19. Franco A. Current perspectives of pediatric PET/MRI. Clin Pediatr. 2019;2:1016.
20. Mannheim JG, Schmid AM, Schwenck J, Katiyar P, Herfert K, Pichler BJ, et al. PET/MRI hybrid systems. Semin Nucl Med. 2018;48:332–47.
21. Bezrukov I, Schmidt H, Gatidis S, Mantlik F, Schäfer JF, Schwenzer N, et al. Quantitative evaluation of segmentation-and atlas-based attenuation correction for PET/MR on pediatric patients. J Nucl Med. 2015;56(7):1067–74.
22. Boxt LM. Magnetic resonance and computed tomographic evaluation of congenital heart disease. J Magn Reson Imaging. 2004;19(6):827–47.
23. Boechat MI, Ratib O, Williams PL, Gomes AS, Child JS, Allada V. Cardiac MR imaging and MR angiography for assessment of complex tetralogy of Fallot and pulmonary atresia. Radiographics. 2005;25(6):1535–46.
24. Purz S, Sabri O, Viehweger A, Barthel H, Kluge R, Sorge I, et al. Potential pediatric applications of PET/MR. J Nucl Med. 2014;55(Supplement 2):32S–9S.
25. Hirsch FW, Sattler B, Sorge I, Kurch L, Viehweger A, Ritter L, et al. PET/MR in children. Initial clinical experience in paediatric oncology using an integrated PET/MR scanner. Pediatr Radiol. 2013;43(7):860–75.
26. Takalkar A, Chen W, Desjardins B, Alavi A, Torigian DA. Cardiovascular imaging with PET, CT, and MR imaging. PET Clin. 2008;3(3):411–34.
27. Rischpler C, Nekolla SG, Dregely I, Schwaiger M. Hybrid PET/MR imaging of the heart: potential, initial experiences, and future prospects. J Nucl Med. 2013;54(3):402–15.
28. Rife E, Gedalia A. Kawasaki disease: an update. Curr Rheumatol Rep. 2020;22(10):75.
29. Friedman KG, Gauvreau K, Hamaoka-Okamoto A, Tang A, Berry E, Tremoulet AH, et al. Coronary artery aneurysms in Kawasaki disease: risk factors for progressive disease and adverse cardiac events in the US population. J Am Heart Assoc. 2016;5(9):e003289.
30. Hernandez-Pampaloni M, Allada V, Fishbein MC, Schelbert HR. Myocardial perfusion and viability by positron emission tomography in infants and children with coronary abnormalities: correlation with echocardiography, coronary angiography, and histopathology. J Am Coll Cardiol. 2003;41(4):618–26.
31. Frommelt PC, Frommelt MA. Congenital coronary artery anomalies. Pediatr Clin North Am. 2004;51(5):1273–88.
32. Gittenberger-de Groot AC, Koenraadt WMC, Bartelings MM, Bökenkamp R, DeRuiter MC, Hazekamp MG, et al. Coding of coronary arterial origin and branching in congenital heart disease: the modified Leiden convention. J Thorac Cardiovasc Surg. 2018;156(6):2260–9.
33. Sithamparanathan S, Padley SPG, Rubens MB, Gatzoulis MA, Ho SY, Nicol ED. Great vessel and coronary artery anatomy in transposition and other coronary anomalies: a universal descriptive and alpha-numerical sequential classification. JACC Cardiovasc Imaging. 2013;6(5):624–30.
34. Click RL, Holmes DR, Vlietstra RE, Kosinski AS, Kronmal RA. Anomalous coronary arteries: location, degree of atherosclerosis and effect on survival—a report from the Coronary Artery Surgery Study. J Am Coll Cardiol. 1989;13(3):531–7.
35. Davis JA, Cecchin F, Jones TK, Portman MA. Major coronary artery anomalies in a pediatric population: incidence and clinical importance. J Am Coll Cardiol. 2001;37(2):593–7.
36. Dodge-Khatami A, Mavroudis C, Backer CL. Anomalous origin of the left coronary artery from the pulmonary artery: collective review of surgical therapy. Ann Thorac Surg. 2002;74(3):946–55.
37. Backer CL, Stout MJ, Zales VR, Muster AJ, Weigel TJ, Idriss FS, et al. Anomalous origin of the left coronary artery. A twenty-year review of surgical management. J Thorac Cardiovasc Surg. 1992;103(6):1049–57; discussion 1057-1058.
38. Azour L, Jacobi AH, Alpert JB, Uppu S, Latson L, Mason D, et al. Congenital coronary artery anomalies and implications. J Thorac Imaging. 2018;33(5):W30–8.
39. Walsh R, Nielsen JC, Ko HH, Sanz J, Srivastava S, Parness IA, et al. Imaging of congenital coronary artery anomalies. Pediatr Radiol. 2011;41(12):1526–35.
40. Hoffman JIE, Kaplan S. The incidence of congenital heart disease. J Am Coll Cardiol. 2002;39(12):1890–900.

41. McElhinney DB, Reddy VM, Silverman NH, Hanley FL. Modified Damus-Kaye-Stansel procedure for single ventricle, subaortic stenosis, and arch obstruction in neonates and infants: midterm results and techniques for avoiding circulatory arrest. J Thorac Cardiovasc Surg. 1997;114(5):718–25; discussion 725-726.
42. Jamar F, Buscombe J, Chiti A, Christian PE, Delbeke D, Donohoe KJ, et al. EANM/SNMMI guideline for 18F-FDG use in inflammation and infection. J Nucl Med. 2013;54(4):647–58.
43. Slart RHJA, Glaudemans AWJM, Gheysens O, Lubberink M, Kero T, Dweck MR, et al. Procedural recommendations of cardiac PET/CT imaging: standardization in inflammatory-, infective-, infiltrative-, and innervation- (4Is) related cardiovascular diseases: a joint collaboration of the EACVI and the EANM: summary. Eur Heart J Cardiovasc Imaging. 2020;21(12):1320–30.
44. Yabrodi M, Hermann JL, Brown JW, Rodefeld MD, Turrentine MW, Mastropietro CW. Minimization of surgical site infections in patients with delayed sternal closure after pediatric cardiac surgery. World J Pediatr Congenit Heart Surg. 2019;10(4):400–6.
45. Jha P, Woodward CS, Gardner H, Pietz C, Husain SA. A quality improvement initiative to reduce surgical site infections in patients undergoing delayed sternal closure after pediatric cardiac surgery. Pediatr Cardiol. 2020;41(7):1402–7.
46. Hariri H, Tan S, Martineau P, Lamarche Y, Carrier M, Finnerty V, et al. Utility of FDG-PET/CT for the detection and characterization of sternal wound infection following sternotomy. Nucl Med Mol Imaging. 2019;53(4):253–62.
47. Pelletier-Galarneau M, Abikhzer G, Harel F, Dilsizian V. Detection of native and prosthetic valve endocarditis: incremental attributes of functional FDG PET/CT over morphologic imaging. Curr Cardiol Rep. 2020;22(9):93.
48. Pizzi MN, Dos-Subirà L, Roque A, Fernández-Hidalgo N, Cuéllar-Calabria H, Pijuan Domènech A, et al. 18F-FDG-PET/CT angiography in the diagnosis of infective endocarditis and cardiac device infection in adult patients with congenital heart disease and prosthetic material. Int J Cardiol. 2017;248:396–402.
49. Partington SL, Valente AM, Landzberg M, Grant F, Di Carli MF, Dorbala S. Clinical applications of radionuclide imaging in the evaluation and management of patients with congenital heart disease. J Nucl Cardiol. 2016;23(1):45–63.
50. Zhang Y, Williams H, Pucar D. FDG-PET identification of infected pulmonary artery conduit following tetralogy of Fallot (TOF) repair. Nucl Med Mol Imaging. 2017;51(1):86–7.
51. Meyer Z, Fischer M, Koerfer J, Laser KT, Kececioglu D, Burchert W, et al. The role of FDG-PET-CT in pediatric cardiac patients and patients with congenital heart defects. Int J Cardiol. 2016;220:656–60.
52. Kouijzer IJE, Mulders-Manders CM, Bleeker-Rovers CP, Oyen WJG. Fever of unknown origin: the value of FDG-PET/CT. Semin Nucl Med. 2018;48(2):100–7.
53. Pijl JP, Kwee TC, Legger GE, Peters HJH, Armbrust W, Schölvinck EH, et al. Role of FDG-PET/CT in children with fever of unknown origin. Eur J Nucl Med Mol Imaging. 2020;47(6):1596–604.
54. Blokhuis GJ, Bleeker-Rovers CP, Diender MG, Oyen WJG, Draaisma JMT, de Geus-Oei L-F. Diagnostic value of FDG-PET/(CT) in children with fever of unknown origin and unexplained fever during immune suppression. Eur J Nucl Med Mol Imaging. 2014;41(10):1916–23.
55. Jeewa A, Imamura M, Canter C, Niebler RA, VanderPluym C, Rosenthal DN, et al. Long-term outcomes after transplantation after support with a pulsatile pediatric ventricular assist device. J Heart Lung Transplant. 2019;38(4):449–55.
56. Absi M, Bocchini C, Price JF, Adachi I. F-fluorodeoxyglucose-positive emission tomography/CT imaging for left ventricular assist device-associated infections in children. Cardiol Young. 2018;28(10):1157–9.
57. Burki S, Adachi I. Pediatric ventricular assist devices: current challenges and future prospects. Vasc Health Risk Manag. 2017;13:177–85.
58. Dell'Aquila AM, Mastrobuoni S, Alles S, Wenning C, Henryk W, Schneider SRB, et al. Contributory role of fluorine 18-Fluorodeoxyglucose positron emission tomography/computed tomography in the diagnosis and clinical Management of Infections in patients supported with a continuous-flow left ventricular assist device. Ann Thorac Surg. 2016;101(1):87–94. discussion 94
59. Mahmood M, Kendi AT, Ajmal S, Farid S, O'Horo JC, Chareonthaitawee P, et al. Meta-analysis of 18F-FDG PET/CT in the diagnosis of infective endocarditis. J Nucl Cardiol. 2019;26(3):922–35.
60. Turpin S, Lambert R, Poirier N. An unusual looking pacemaker infection imaged with 18F-FDG PET/CT. Eur J Nucl Med Mol Imaging. 2010;37(7):1438.
61. Chiabrando JG, Bonaventura A, Vecchié A, Wohlford GF, Mauro AG, Jordan JH, et al. Management of acute and recurrent pericarditis: JACC state-of-the-art review. J Am Coll Cardiol. 2020;75(1):76–92.
62. Kim M-S, Kim E-K, Choi JY, Oh JK, Chang S-A. Clinical utility of [18F]FDG-PET/CT in pericardial disease. Curr Cardiol Rep. 2019;21(9):107.
63. Martineau P, Dilsizian V, Pelletier-Galarneau M. Incremental value of FDG-PET in the evaluation of cardiac masses. Curr Cardiol Rep. 2021;23(7):78.
64. Bligh MP, Borgaonkar JN, Burrell SC, MacDonald DA, Manos D. Spectrum of CT findings in thoracic extranodal non-Hodgkin lymphoma. Radiographics. 2017;37(2):439–61.
65. Gerardin C, Mageau A, Benali K, Jouan F, Ducrocq G, Alexandra J-F, et al. Increased FDG-PET/CT peri-

cardial uptake identifies acute pericarditis patients at high risk for relapse. Int J Cardiol. 2018;271: 192–4.
66. Dong A, Dong H, Wang Y, Cheng C, Zuo C, Lu J. (18) F-FDG PET/CT in differentiating acute tuberculous from idiopathic pericarditis: preliminary study. Clin Nucl Med. 2013;38(4):e160–5.
67. Pelletier-Galarneau M, Martineau P, Zuckier LS, Pham X, Lambert R, Turpin S. 18F-FDG-PET/CT imaging of thoracic and extrathoracic tuberculosis in children. Semin Nucl Med. 2017;47:304–18.
68. Chang SA, Oh JK. Constrictive pericarditis: a medical or surgical disease? J Cardiovasc Imaging. 2019;27(3):178–86.